



A novel impedimetric sensor based on CuO(NPs)/polyaniline/murexide composite for cholesterol detection

Chedia Ben Ali Hassine¹ · Hamza Kahri¹ · Houcine Barhoumi¹

Received: 28 March 2021 / Accepted: 10 September 2021 / Published online: 23 September 2021
© Iranian Chemical Society 2021

Abstract

In this study, we report a novel non-enzymatic cholesterol biosensor based on copper oxide nanoparticles (CuO), polyaniline nanofibers (PANI) and murexide (Mu) modified glassy carbon electrode. The modified electrode was used for the detection of cholesterol. Copper oxide nanoparticles were deposited on the glassy carbon electrode through electrodeposition and electrochemical oxidation followed by electrodeposition of PANI–Mu composite. The prepared GC/CuO(NPs)/PANI/Mu sensor was characterized using electrochemical, optical and morphological methods such as cyclic voltammetry (CV), impedance spectroscopy (EIS), linear sweep voltammetry (LSV), UV–visible and scanning electron microscopy (SEM). The electrochemical response of the elaborated composite matrix for cholesterol detection was evaluated by employing the impedance spectroscopy method. The results were promising as we obtained good analytical performances for cholesterol quantification with high sensitivity of 5575 $\Omega/\log M$, a wide linear range from 0.5 to 50 mM and a low detection limit of 1 nM.

Keywords Glassy carbon electrode · Polyaniline · Murexide · Cholesterol detection · Impedance spectroscopy, Voltammetry

Introduction

Cholesterol is an organic molecule; it belongs of the sterol family (Fig. 1) [1]. Cholesterol is one of the most constituents of mammalian cell membranes further cholesterol molecule is known as precursor of other biological materials [2]. Cholesterol is an important structural component of the plasma membrane, where it maintains a barrier between cells and the environment also it regulates the permeability and the fluidity. Cholesterol is the main substrates for the synthesis of steroid hormones, bile acids and vitamin D. An insufficient supply of cholesterol produces detrimental effects on cell function, tissue development and body physiology. Nevertheless, a high level of cholesterol in blood can cause pathological consequences [3].

The detection of cholesterol has received a lot of interest because high cholesterol blood levels can increase risks of heart diseases like atherosclerosis, high blood pressure and myocardial infraction [4]. As a result, most food producers

are obliged to decrease the cholesterol level in food in order to control cardio-diseases. Therefore, there is an increasing demand for sensitive, selective, fast, inexpensive and robust methods for cholesterol determination in food [5]. The progress in non-enzymatic electrochemical detection of cholesterol was highly accelerated according to the innovative and powerful new sensing material such as nanoparticles and conductive polymers [6–8]. Nanocomposites have attracted a lot of attention due to their unique physical properties and wide range of applications. Polymer nanocomposites have captivated scientists considering their novel properties gathered from the successful combination of the characteristics of many constituents into a single material [9]. Recently, conducting polymers get a lot a consideration especially polyaniline (PANI). PANI is characterized as air stable organic polymer, high electrical conductivity, good environmental, chemical, electrical stability and simple synthesis [10, 11]. The utilization of nanoparticles like copper oxide (CuO), a versatile semiconductor material, has been attracting the attention due to the commercial demand for electronic devices. Copper oxide has recently been used in several research due to its fascinating properties and wide range of applications such as heterogeneous catalysts, gas sensors, superconductors, lithium ion electrode materials,

✉ Hamza Kahri
hamza.kahri@bilkent.edu.tr

¹ Laboratory of Interfaces and Advanced Materials, Faculty of Sciences, University of Monastir, Monastir, Tunisia

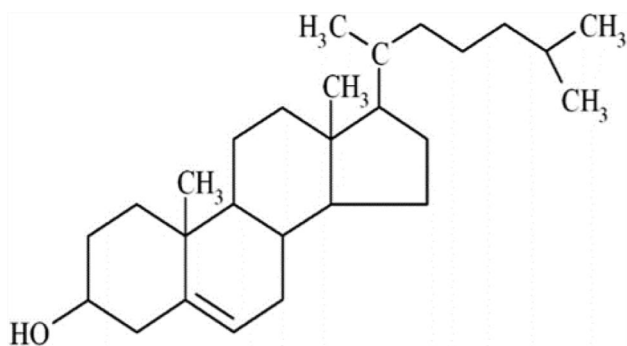


Fig. 1 Cholesterol chemical structure

solar cells and sensors [12–14]. CuO nanostructures have been used as an active material for the elaboration of electrochemical sensors for the reason that they have excellent catalytic and electrochemical properties, low temperature and inexpensive [15, 16]. The development of inorganic/organic hybrid materials on nano-meter scale have received significant attention thanks to their unique properties [17, 18]. Overall, the synthesis of hybrid nanocomposites based on polymer and inorganic materials forms a new composite material having synergetic or complementary behaviors of the polymer and the inorganic material [19, 20]. Murexide is the ammonium salt of purpuric acid, it has the appearance of a reddish purple powder and is used in analytical chemistry [21, 22]. Murexide contributed to the biocompatibility of the sensor, better dispersion and hydrophilic properties by introducing more hydroxyl groups. The hydroxyl groups compensated the positive charges on polymer chains and suppressed the deprotonation processes [23]. During this study, a modified electrode based on polyaniline nanostructures, CuO nanoparticles and murexide molecules was developed for the impedimetric detection of cholesterol.

Material and methods

Reagents

Copper sulfate pentahydrate $\text{CuSO}_4(5\text{H}_2\text{O})$, Potassium monohydrogen phosphate (K_2HPO_4) and Potassium dihydrogen phosphate (KH_2PO_4) were purchased from Fluka (French). KCl (potassium chloride) was purchased from PROLABO. Aniline was purchased from Sigma-Aldrich (Tunisia). Cholesterol was purchased from Alfa Aesar (Tunisia). Hydroquinone, sulfuric acid, triton-X-100 and murexide were purchased from Merck (Tunisia). Chemicals were of analytical grade and were used without further

purification. Aqueous solutions were prepared using distilled–deionised water using a water distillatory and water deionizer in a second time.

Apparatus

Electrochemical data were obtained in a standard three-electrode cell using a potentiostat (DY200 POT Eco-chimie/Moldova) and an Autolab PGSTAT 320 N potentiostat/galvanostat (Metrohm/Switzerland). An electrode made of glassy carbon with a 3 mm diameter was used as a working electrode. The counter electrode used was a platinum (Pt) wire. The reference electrode was an Ag/AgCl(KCl) electrode. For the PANI–Mu electrodeposition a saturated calomel electrode (S.C.E) was used. Permeability measurements are performed on a rotating working electrode. The UV–Visible measurements were carried out in a spectrophotometers models 6705 UV/Vis (JENWAY/UK). The morphological characterization of the modified electrodes was carried out by a scanning electron microscope JSM 5100 from JEOL/USA using carbon screen-printed electrode. Cholesterol solutions were freshly prepared using deionized water and 10% triton-X-100. Cholesterol detection was done with impedimetric measurement in phosphate buffered solution, pH=7.4.

Electrode modification

The first step, was the working electrode cleaning by polishing using 0.3 μm alumina powders then sonicated and rinsed with deionized water. The second step was the electrochemical activation in NaOH 0.5 M at a scan rate of 50 $\text{mV}\cdot\text{s}^{-1}$ employing several cycles in the range of 0.6 to 1.2 V. Figure 1 shows the different steps adopted for the elaboration of the modified electrode. In brief, the cleaned and activated working electrode was dried before use. The Cu nanoparticles were electrodeposited on the working electrode surface at a constant potential of -0.6 V. Following this step, in order to obtain copper oxide nanoparticles (Cu_xO) (Fig. 2A), cyclic voltammetry was performed in NaOH solution (0.1 M) at the applied potential range from -0.5 to 0.3 V with a scan rate of 50 $\text{mV}\cdot\text{s}^{-1}$ for 40 cycles [24]. As given in Fig. 2A, we observe a decrease in the intensity of the peak which appears toward -0.15 V indicating the formation of CuO nanoparticles. An electrolyte containing H_2SO_4 and aniline was used for the electrodeposition of PANI nanofibers on the electrode [25]. PANI–Mu composite was prepared by chronoamperometry at $U=0.85$ V versus SCE for 1500 s in 1.00 M H_2SO_4 solution containing 0.025 M aniline and 0.00125 M murexide. As shown in Fig. 2B, during the first stage (from 0 to 500 s), the current density increases sharply then increased slowly from 500 to 1600 s.

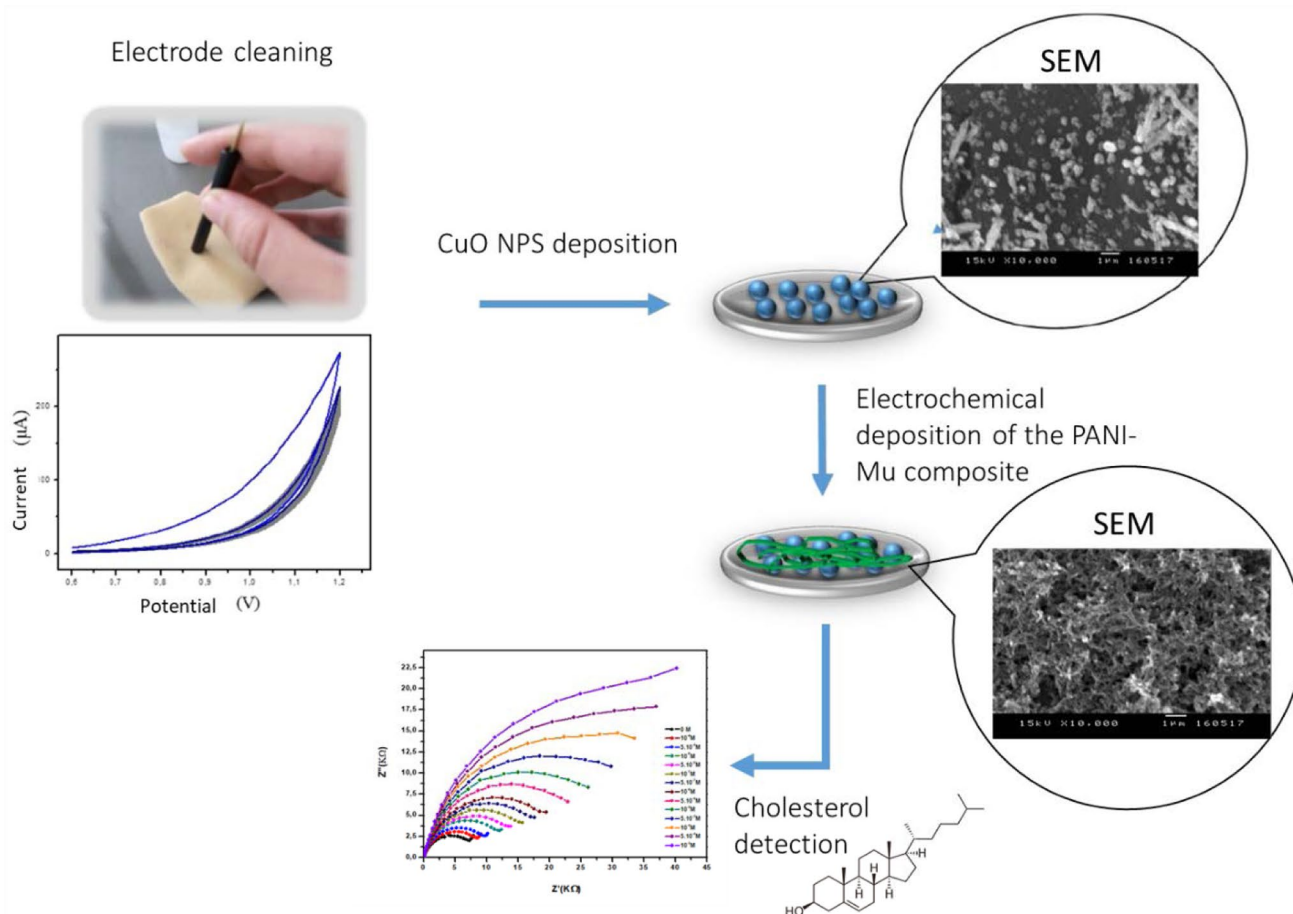


Fig. 2 Schematic illustration of the experimental process during sensor fabrication

Results and discussions

Electrode characterization

The characterization of bare and modified GC electrodes was investigated by cyclic voltammetry (CV), electrochemical impedance spectroscopy (EIS), linear sweep voltammetry (LSV) measurements and scanning electron microscopy (SEM). In order to characterize the formation of the composite layer on the GC electrode surface, CV were applied in the presence of hydroquinone 10^{-3} M in phosphate buffer solution (PBS) at pH = 7.4. Figure 3 shows the cyclic voltammograms recorded for the modified and the bare electrodes. The electron transfer is more efficient at modified electrodes if compared with the bare GC electrode. An increase in anodic and cathodic current response is observed after electrode modification indicating that the modified electrode surface was electrochemically active. The anodic peaks for bare GC, GC/Cu(NPs), GC/CuO(NPs), GC/CuO(NPs)/PANI and GC/CuO(NPs)/

PANI/Mu electrodes, respectively, are 108, 130, 112, 120 and $88\mu\text{A}$. A decrease in the anodic current is observed after the addition of Mu. According to Fig. 3, a shift in the oxidation potential of hydroquinone is observed with an increase in the potential difference (ΔE) from 90 to 400 mV after modification of the electrode surface. The impedance measurements were employed to investigate the modification effect of the electrodes surfaces. Figure 4A represents typical Nyquist plots for bare GC, GC/Cu(NPs), GC/CuO(NPs), GC/CuO(NPs)/PANI and GC/CuO(NPs)/PANI/Mu electrodes. The Nyquist plots of the bare electrode represents at low frequency a straight line with a small semi-circle at high frequency region. On the opposite hand, the Nyquist plots of the modified electrodes represents a semi-circle at high frequency region, which is expounded to higher charge transfer resistance (R_{ct}) than it was estimated for the bare GCE. The variation indicates the passivation of the GC electrode. To simulate the Nyquist plots, a standard Randles equivalent circuit was used to estimate the analytical parameters as presented

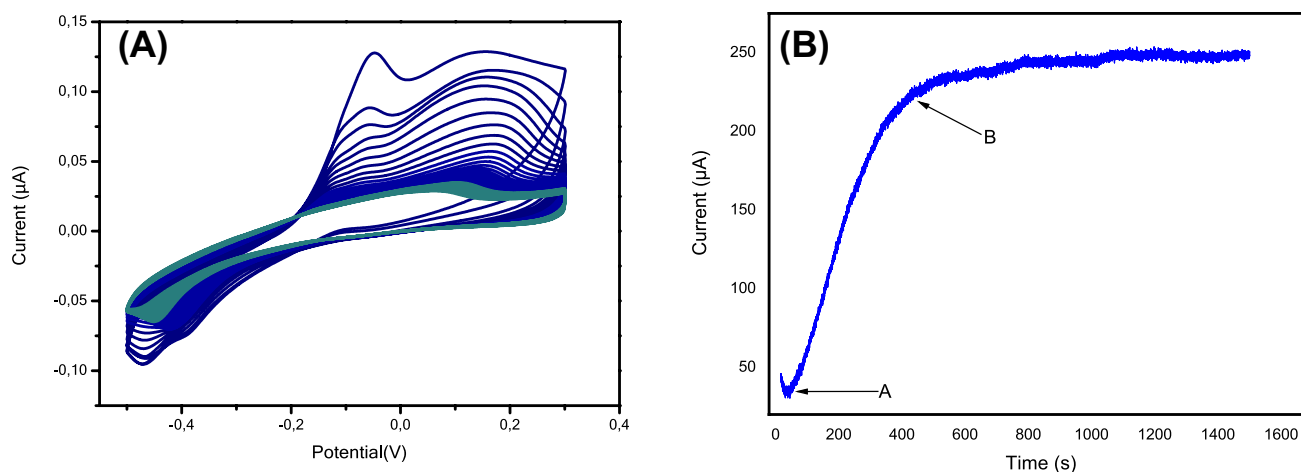


Fig. 3 (A) Oxidation of copper nanoparticles by cyclic voltammetry in 0.1 M NaOH solution (40 cycles, 50 mV/s) and (A) Chronoamperometry at $U = 0.85$ V versus SCE for 1500 s in 1.00 M H_2SO_4 solution containing 0.025 M aniline and 0.00125 M murexide

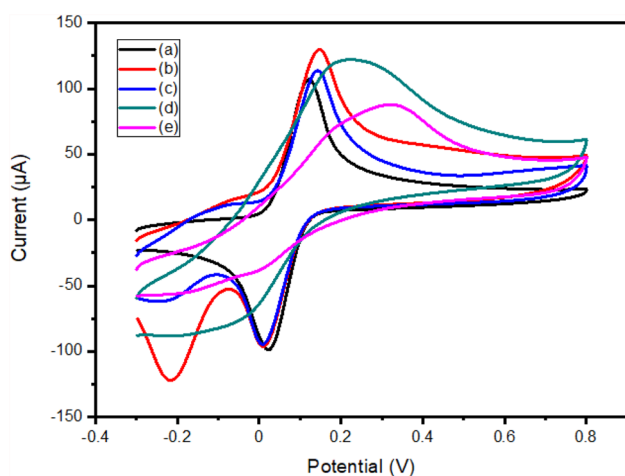


Fig. 4 Cyclic voltammograms of different modified electrodes performed with hydroquinone 10^{-3} M in Pbs pH=7.4. At potential sweep rate of 100 mV/s vs. Ag/AgCl/(sat. KCl). **a** Bare GCE, **b** GCE/Cu(NPs), **c** GCE/CuO(NPs), **d** GCE/CuO(NPs)/PANI and **e** GCE/CuO(NPs)/PANI/Mu

in Fig. 4B. The proposed equivalent circuit includes the solution resistance (R_s), the charge transfer resistance (R_{ct}), the Warburg impedance (W_o) and the constant phase element (CPE). The experimental impedance values are coupled with Randles equivalent circuit simulation using

Nova software. The electrode coverage rate was calculated using the relation given by Eq. (1) [25, 26].

$$\theta = 1 - \frac{R_{ct}^0}{R_{ct}} \quad (1)$$

, where R_{ct}^0 is the charge transfer resistance of the bare GC electrode and R_{ct} is the charge transfer resistance of the modified electrode. The obtained results from Eq. (1) are gathered in Table 1. Using the variation of charge transfer resistance after the formation of the CuO(NPs)/PANI/Mu film, it can be deduced that the coverage rate is 86%. In fact, when the electrode modification was performed, a dense and better-packed layer of CuO(NPs)/PANI/Mu was established. Therefore, it could be concluded that nanoparticles were intercalated in the conducting polymer film. The permeability P_m of the elaborated films under optimal conditions was investigated using a rotating disk electrode (RDE) as shown in Figs. 5A. The rotating disk voltammograms were recorded for the modified electrodes at different rotation rates in an aqueous solution of hydroquinone as electroactive permanent and compared to the results obtained from a bare glassy carbon electrode. An increase is observed with the increase of the rpm from 200 to 1200 rpm. The calculation was done according to the equation introduced by Gough and Leypoldt [27]. The equation relates the variation of limiting current i_{lim} with the mass transport for a functionalized rotating disk electrode [28]. P_m was calculated using this equation:

$$\frac{1}{i_{lim}} = \frac{1}{0.62} \times n \times F \times A \times D_s^{2/3} \times C^0 \times v^{-1/6} \times w^{1/2} + \frac{1}{nF} P_m \times A \times C^0, \quad (2)$$

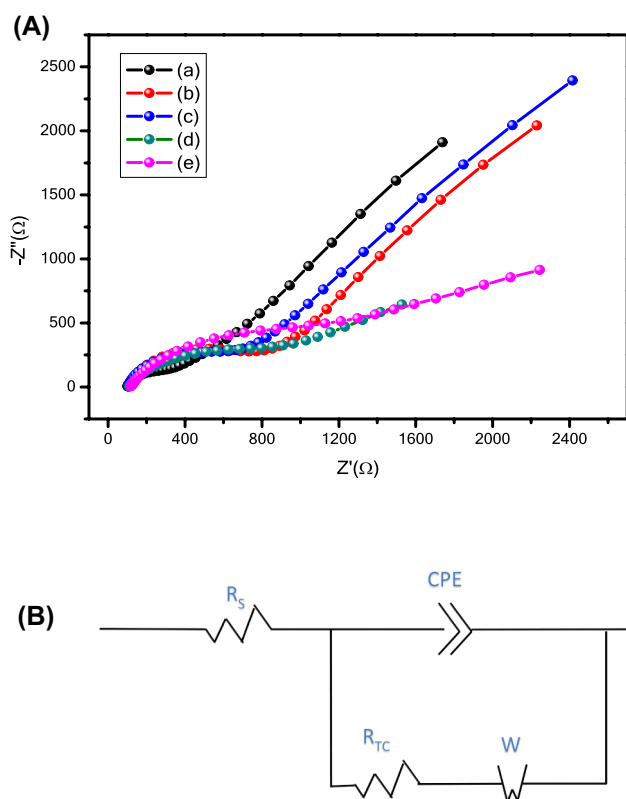


Fig. 5 (A) Nyquist plots of the modified electrodes performed with hydroquinone (10^{-3} M) in Pbs pH=7.4 solution. (a) Bare GCE, (b) GCE/Cu NPs, (c) GCE/CuO(NPs), (d) GCE/CuO (NPs)/PANI and (e) GCE/CuO(NPs)/PANI/Mu. Frequency range is from 0.05 to 75,000 Hz, the modulation amplitude is 10 mV and the working electrode potential is 250 mV. (B) Randle-type equivalent circuit

Table 1 Simulation parameters of the modified electrode using Nyquist diagrams. The used circuit is [(R (Q [RW])]

Matrix	$R_s(\Omega)$	$R_{TC}(\Omega)$	$\Theta\%$
Bare GCE	103.61	177.43	–
GCE/Cu NPs	109.59	541.49	67
GCE/CuO NPs	105.66	432.97	59
GCE/CuO NPs/PolyAN	111.62	823.01	78
GCE/CuO NPs/PolyAN + Mu	108.01	1275.9	86

where n is the number of electrons transferred, F is the Faraday constant, A is the electrode radius, D is the diffusion coefficients for the substrate in the bulk solution, C is the hydroquinone concentration, ν is the kinematic viscosity of the solution and ω is the rotation rate of the RDE. The plot of $1/i_{lim}$ versus $\omega^{1/2}$ presents a linear behavior with a positive intercept that depends on the permeability P_m of the film (Fig. 5B). Permeability values of 0.0039 and 0.0027 $\text{cm}\cdot\text{s}^{-1}$ were calculated for the GC/CuO(NPs)/PANI and the GC/CuO(NPs)/PANI/Mu electrodes, respectively. According

to these values we can assume that the deposited film is permeable to some molecules. UV visible spectroscopy was done to evaluate the optical activity of the developed film. Figure 6 shows the spectra of the PANI layer containing two distinctive peaks at 326 nm and 644 nm which are attributed to π - π^* and polaron- π^* transitions, respectively [29]. The UV-visible spectra of the composite film present three distinctive peaks localized at 259 nm, 292nm and 452 nm which can be assigned to n - π^* for nanocomposite, π - π^* transition of benzenoid and π - π^* transition of quinoid, respectively. From literature [17] and Fig. 6, it is affirmed that the characteristic peaks of PANI, Mu and CuO(NPs) appeared in the CuO(NPs)/PANI/Mu composite. Moreover, peaks of polyaniline, CuO(NPs) and Mu at nanocomposite are obviously shifted to shorter wavelength. It is important to mention that the use of CuO(NPs) as a doping agent in the polymer matrix generates displacements in the bands of PANI spectra due to the interaction of NPs with polyaniline. The SEM images of bare GC, SPCE/CuO(NPs), SPCE/CuO(NPs)/PANI and SPCE/CuO(NPs)/PANI/Mu electrodes surfaces are gathered in Fig. 7. According to Fig. 7, it is clear that the bare and modified electrodes surfaces are different from each other. Figure 7b shows the formation of CuO (NPs) on the electrode surface. The same procedure of deposition was used in a previous work in order to elaborate CuO(NPs) [24]. The SEM image in Fig. 7(c and d) shows that polymeric layer is uniformly distributed on the electrode surface. The layer is composed of PANI nanofibers as it can be seen in Fig. 7 and as discussed by Haibin Zhang and all [30]. They estimate that the applied potential resulted in different PANI morphologies. This phenomenon can be attributed to the decomposition of PANI controlled by potentials. As we know, the decomposition of PANI occurred simultaneously with the polymerization and there is a competition between the polymerization and the decomposition. The electrochemical polymerization of aniline involves two stages. An initial stage, PANI grew on the bare electrode and a second stage, PANI grew more on the electrode surface creating a compact PANI layer [20]. These two stages can be observed in Fig. 7 (Stage A and B). When the applied potentials reached 1.00 V versus SCE, the decomposition of PANI was not negligible. However, in present experiments, the applied potentials did not exceed 0.85 V versus SCE, and the decomposition of PANI can be neglected. Therefore, the PANI nanofibers can be obtained easily [31]. From the SEM image, we can observe better fibers using murexide molecules.

Electrochemical performances of the sensing matrix for cholesterol quantification

The deposited CuO (NPs)/PANI/Mu composite layer was used for cholesterol detection using electrochemical

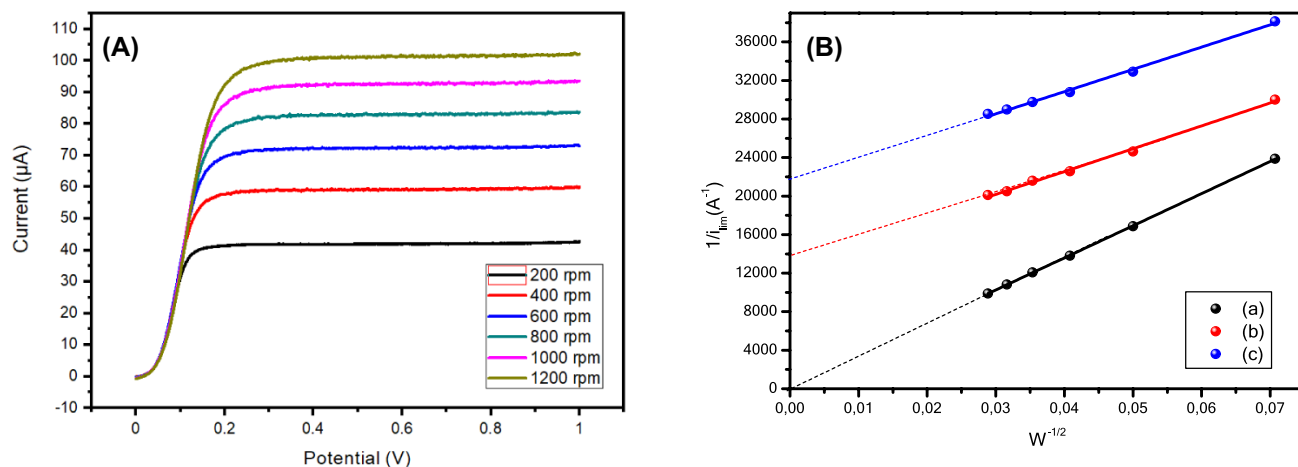


Fig. 6 Spectrum of linear voltammograms **(A)** and Koutecky–Levich characteristics **(B)** of **(a)** Bare GCE, **(b)** GCE/CuO(NPs)/PANI, **(c)** GCE/CuO(NPs)/PANI/Mu ($V = 10 \text{ mV/s}$, 1 mM Hydroquinone in phosphate buffer $\text{pH} = 7.4$). $W^{1/2}$ is in $(\text{Rad/s})^{1/2}$

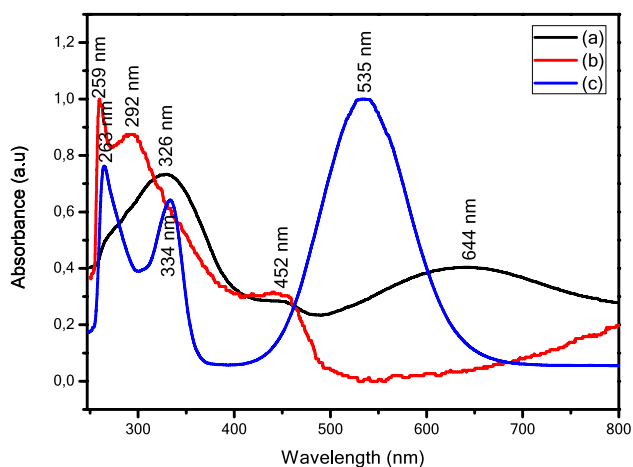


Fig. 7 UV–visible spectra for **a** PANI, **b** CuO(NPs)–PANI–Mu nano-composite film and **c** Mu

impedance spectroscopy measurements (Fig. 8). Impedance parameters were calculated with NOVA software and fitting the obtained diagrams. An increase in charge transfer resistance (R_{ct}) is observed with the increase of cholesterol concentration in the solution. A decrease in Warburg values with increasing cholesterol concentration. These changes in impedance parameters indicate the electrode passivation. A significant increase in the charge transfer resistance as a function of cholesterol concentration is observed. The calculation of the surface coverage of the electrode after each addition shows an increase in the covered electrode surface

from 9 to 83%. This increase proves that cholesterol molecules adhere to the surface of the electrode and increases its concentration in the solid–liquid interface. The cholesterol adhesion on the electrode surface is probably due to its hydrophobic property [32]. Figure 9 shows the plot of R_{ct} as a function of $-\log[\text{cholesterol}]$. The modified electrode showed a linear relationship between the charge transfer resistance and the cholesterol concentration in the range from 50 to 0.5 nM ($y = -5575 \times x + 54,700$ ($R^2 = 0.9780$)). The deposited layer presents a good sensitivity of $5575 \Omega/\log M$ for cholesterol detection. These results indicated that the modified electrode has excellent ability for non-enzymatic detection of cholesterol if compared with previous reports as shown in Table 2. For a non-enzymatic cholesterol sensor, the selectivity is a crucial parameter. It is well known that ascorbic acid (AA), uric acid (UA) and glucose interfere with the detection of cholesterol [33]. Therefore, in this study, concentrations of these molecules are 10 times higher than cholesterol concentration. The response of the sensor was recorded in the sample solution containing 10^{-5} M of cholesterol. Figures 10 and 11 summarizes the results obtained indicating a small variation of the charge transfer resistance in presence of the studied interfering compounds. 0.68%, 6% and 8% in the signal were observed for glucose, AA and UA, respectively. The applicability of the elaborated cholesterol sensor was verified by the determination of the amount of cholesterol in milk samples. Specifically, milk samples were diluted with PBS (0.1 M) and a known

Fig. 8 Scanning electron micrographs of **a** bare screen-printed carbon electrode (SPCE), **b** SPCE/CuO(NPs), **c** SPCE/CuO(NPs)/PANI and **d** SPCE/CuO(NPs)/PANI/Mu. Resolution of 1 μm , magnification of 10,000 and accelerating potential of 15.0 kV were used

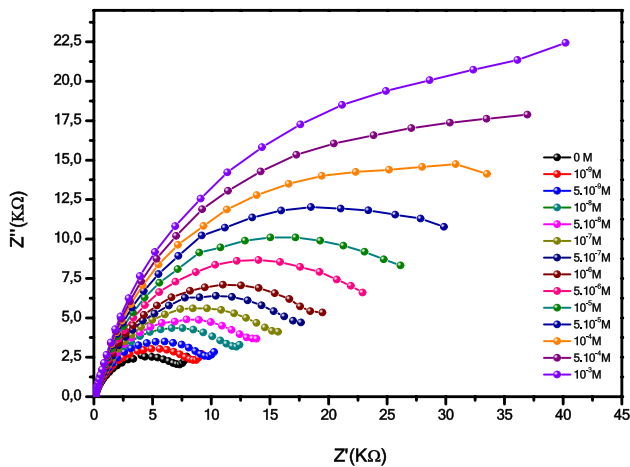
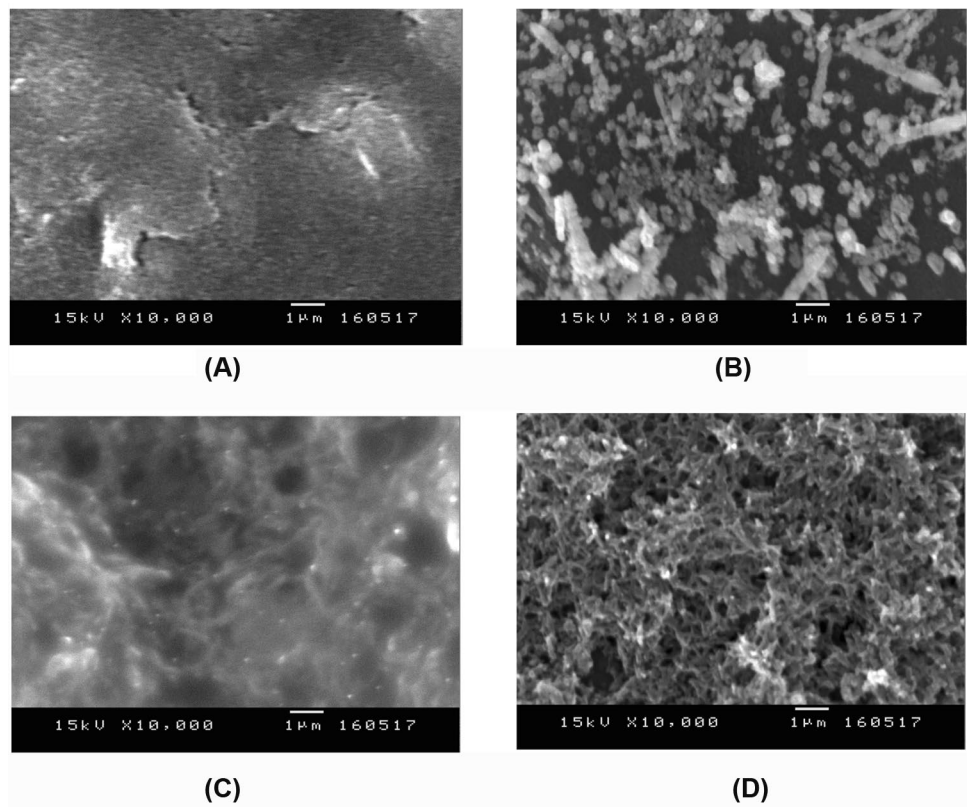


Fig. 9 Nyquist diagrams corresponding to the detection of different concentrations of Cholesterol ranging from 10^{-9} to 10^{-3} M in phosphate buffer solution (100 mM) pH = 7.4

cholesterol concentration was added to the solution. No further treatment of the sample was required. The obtained results are summarized in Table 3, which indicates that the elaborate sensor show a good quantification of cholesterol in milk samples.

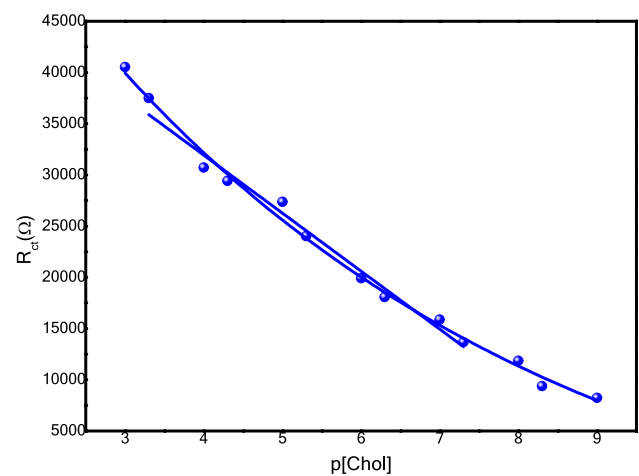


Fig. 10 Linear relationship between R_{ct} and the negative logarithm of cholesterol concentration

Conclusion

A CuO(NPs)/PANI/Mu nanocomposite deposited onto a glassy carbon electrode was used to investigate the non-enzymatic detection of cholesterol. The SEM analysis showed that CuO (NPs) were incorporated onto the polyaniline–murexide composite. The electrochemical response for

Table 2 Comparison of the results of the present study with previous reports for cholesterol sensing

Matrix	Method	Detection limit	Linear range	Sensitivity	Refs.
NiO nanorods	Cyclic voltammetry	0.65 mM	0.64–10.3 mM	120 mA.mM ⁻¹	[32]
NiO/CVD-grown graphene	Chronoamperometry	0.13 mM	2–40 mM	40.6 mA mM ⁻¹ cm ⁻²	[33]
Graphene/CD	Differential pulse voltammetry (DPV)	1 mM	0.005–0.03 mM	0.01 mA mM ⁻¹	[34]
Ag/CHOx/Au NPs/SPE	anodic stripping voltammetry (ASV)	3.0 µg/mL	5–5000 µg/mL	0.0610 µA.mL.µg ⁻¹	[35]
Graphene/β-CD/Rhodamine 6G	Fluorescence	–	0.005–0.03 mM	1 µM	[36]
Au-SPE/Pt/PDA-ChOx	Amperometry	10.5 µM	35.3–500 µM	14.3 mA M ⁻¹ cm ⁻²	[37]
ChOx/AuPt-Ch-IL/GCE	Amperometry	10 µM	0.05–6.2 mM and 6.2– 11.2 mM	90.7	[38]
GCE/CuO NPs/PolyAN + Mu	EIS	1 nM	0.5 nM-50 mM	5575 Ω/logM	This work

CVD: Chemical vapor deposition technique

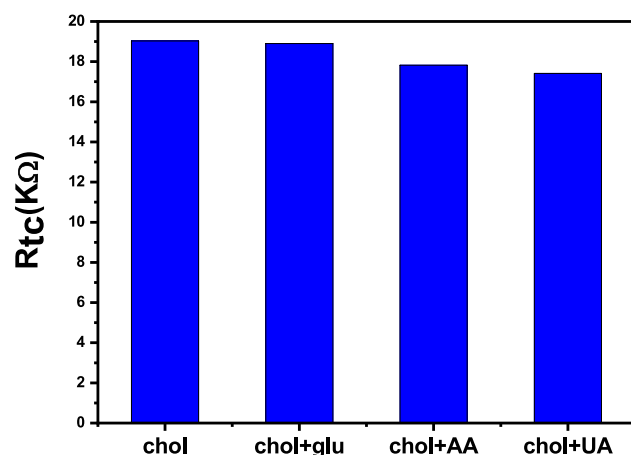
CD: cyclodextrin

SPE: Screen-printed electrode

CHOx: Cholesterol oxidase

PDA: Polydopamine

Ch-IL: Ionic liquid–chitosan composite

**Fig. 11** Interference effect on the charge transfer resistance**Table 3** Cholesterol determination in milk samples

Samples	Added concentration (M)	Measured concentration (M)	%RSD	Recovery %
1	10 ⁻⁸	1.2 × 10 ⁻⁸	1.6	120
2	2 × 10 ⁻⁸	2.15 × 10 ⁻⁸	1.4	107.5
3	4 × 10 ⁻⁸	4.26 × 10 ⁻⁸	1.8	106.5
4	6 × 10 ⁻⁸	6.3 × 10 ⁻⁸	2.3	105

cholesterol quantification was evaluated by Impedance spectroscopy method. The non-enzymatic sensor demonstrates a high sensitivity and good stability in a wide range of concentrations from 0.5 to 1 mM. The developed bioanalytical

system was successful applied for cholesterol determination in milk with high recovery and selectivity.

Acknowledgements Authors would like to acknowledge PRF-2017-D4P1/ Tunisia project (No. 12Mag088), and the Ministry of Higher Education and Scientific Research of Tunisia (LR11ES55). H.K thanks to the Scientific and Technological Research Council of Turkey (TUBITAK) for the fellowship.

Declarations

Conflict of interest There are no conflicts of interest to declare.

References

- S.M. Pourmortazavi, Z. Saghafi, A. Ehsani, M. Yousef, Application of supercritical fluids in cholesterol extraction from food-stuffs: a review, *J. Food Sci. Technol.* **55**, 2823 (2018) <https://doi.org/10.1007/s13197-018-3205-z>
- Y. Lee, J. Park, *Biosens. Bioelectron.* **26**, 1358 (2010)
- D. Mozaffarian, E.J. Benjamin, A.S. Go, D.K. Arnett, M.J. Blaha et al., Executive summary: heart disease and stroke statistics–2016 update: a report from the American Heart Association. *Circulation* **133**, 454 (2016). <https://doi.org/10.1161/CIR.0000000000000350>
- M. Srivastava, S.K. Srivastava, N.R. Nirala, R. Prakash, *Anal. Method.* **6**, 824 (2014). <https://doi.org/10.1039/C3AY41812J>
- K. Derina, E. Korotkova, Y. Taishibekova, L. Salkeeva, B. Kratochvil, J. Barek, *Anal. Bioanal. Chem.* **410**, 5092 (2018). <https://doi.org/10.1007/s00216-018-1164-x>
- G. Li, J. Zeng, Z. Zhao, C. Wang, J. Dong, Z. Liang, Y.H. Zhou, *J. Nanopart. Res.* **162**, 16 (2019). <https://doi.org/10.1007/s11051-019-4602-6>
- Y. Zhang, Y.N. Wang, X.T. Sun, L. Chen, Z.R. Xu, *Sens. Act. B Chem.* **246**, 126 (2017). <https://doi.org/10.1016/j.snb.2017.02.059>

8. S. Gilbert, H.K. Jeong, P.A. Dowben, *Chem. Phys. Lett.* **687**, 226 (2017). <https://doi.org/10.1016/j.cplett.2017.09.024>
9. M.A. Chougule, S. Sen, V.B. Patil, *Synth. Met.* **162**, 1603 (2012). <https://doi.org/10.1016/j.synthmet.2012.07.002>
10. M.J. Sailor, E.J. Ginsburg, C.B. Gorman, A. Kumar, R.H. Grubbs, N.S. Lewis, *Science* **249**, 1149 (1990). <https://doi.org/10.1126/science.249.4973.1146>
11. S.L. Patil, S.G. Pawar, M.A. Chougule, B.T. Raut, P.R. Godse, S. Sen, V.B. Patil, *Int J Polym Mater.* **61**, 820 (2012). <https://doi.org/10.1080/00914037.2011.610051>
12. Y.F. Lim, J.J. Choi, T. Hanrath, *J Nanomater.* **6**, 6 (2012). <https://doi.org/10.1155/2012/393160>
13. X.M. Miao, R. Yuan, Y.Q. Chai, Y.T. Shi, Y.Y. Yuan, *J. Electroanal. Chem.* **612**, 167 (2008). <https://doi.org/10.1016/j.jelechem.2007.09.026>
14. G. Ren, D. Hu, E.W.C. Cheng, M.A. Vargas-Reus, P. Reip, R.P. Allaker, *Int. J. Antimicrob. Agents.* **33**, 590 (2009). <https://doi.org/10.1016/j.ijant.2019.e01878>
15. G. Zhu, H. Xu, Y. Xiao, Y. Liu, A. Yuan, X. Shen., *ACS Appl. Mater. Interfaces.* **4**, 751 (2012). <https://doi.org/10.1021/am2013882>
16. P. Deka, B. J. Borah, H. Saikia, P. Bharali., *The Chemical Record.* **19**, 473 (2019). <https://doi.org/10.1002/tcr.201800055>
17. H. Razmi, H. Nasiri, R. M., *Microchim Acta* **173**, 64 (2011). <https://doi.org/10.1007/s00604-010-0527-6>
18. V. Gautam, K.P. Singh, V.L. Yadav, *Anal. Bioanal. Chem.* **410**, 2181 (2018). <https://doi.org/10.1007/s00216-018-0880-6>
19. C. Sanchez, B. Julian, P. Belleville, M. Popall, *J. Mater. Chem.* **15**, 36 (2005). <https://doi.org/10.1039/B509097K>
20. A. Rengaraj, Y. Haldorai, Ch.H. Kwak, S. Ahn, K.J. Jeon, S.H. Park, Y.K. Han, Y.S. Huh, *J. Mater. Chem. B.* **3**, 6309 (2015). <https://doi.org/10.1039/C5TB00908A>
21. M.S. Masoud, T.S. Kassem, M.A. Shaker, A.E. Al, *J. Therm. Anal. Calorim.* **84**, 555 (2006). <https://doi.org/10.1007/s10973-005-9991-3>
22. K.R. Mahanthesha, B.E. Kumara Swamy, U. Chandra, S. Sharath Shankar, K.V. Pai, *J. Mol. Liq.* **172**, 124 (2012). <https://doi.org/10.1016/j.molliq.2012.05.015>
23. P. Mn Woi, P. M. F. Lorestani, M.R. Mahmoudian, Y. Alias, *Sensor Actuator B Chem.* **209**, 108 (2015). <https://doi.org/10.1016/j.snb.2014.11.072>
24. H. Zhang, J. Wang, Z. Wang, F. Zhang, S. Wang, *Synth. Met.* **159**, 281 (2009). <https://doi.org/10.1016/j.synthmet.2008.09.015>
25. R.P. Janek, W.R. Fawcett, *Langmuir* **14**, 3018 (1998). <https://doi.org/10.1021/la970980+>
26. H. Barhoumi, A. Maaref, M. Rammah, C. Martelet, N. Jaffrezic-Renault, C. Moustyc, S. Cosnier, E. Perezd, I. Rico-Lattes *Biosensor Bioelectron.* **20**, 2323 (2005). <https://doi.org/10.1016/j.bios.2004.10.010>
27. D.A. Gough, J.K. Leyboldt, *Membrane-covered, rotated disk electrode.* *Anal. Chem.* **51**, 444 (1979). <https://doi.org/10.1021/ac50039a028>
28. D.M. Jundale, S.T. Navale, G.D. Khuspe, D.S. Dalavi, P.S. Patil, V.B. Patil, *J Mater Sci: Mater Electron.* **24**, 3535 (2013). <https://doi.org/10.1007/s10854-013-1280-5>
29. L.W. Zhi, L.Y. Qin, *Sensor Actuator B.* **141**, 153 (2009). <https://doi.org/10.1016/j.snb.2009.05.037>
30. Md.A. Ali, P.R. Solanki, M.K. Patel, H. Dhayani, V.V. Agrawal, R. John, B.D. Malhotra, *Nanoscale* **5**, 2891 (2013). <https://doi.org/10.1039/C3NR33459G>
31. N. Agnihotri, A.D. Chowdhury, A. De, *Biosens. Bioelectron.* **63**, 217 (2015). <https://doi.org/10.1016/j.bios.2014.07.037>
32. S. Aravamudhana, A. Kumar, S. Mohapatra, S. Bhansali, *Biosens. Bioelectron.* **22**, 2294 (2007). <https://doi.org/10.1016/j.bios.2006.11.027>
33. A. Rengaraj, Y. Haldorai, C.H. Kwak, S. Ahn, K.J. Jeon, S.H. Park, Y.K. Han, Y.S. Huh, *J. Mater. Chem. B* **3**, 6309 (2015). <https://doi.org/10.1039/C5TB00908A>
34. N. Agnihotri, A.D. Chowdhury, A. De *Biosens, Bioelectron.* **63**, 217 (2015). <https://doi.org/10.1016/j.bios.2014.07.037>
35. Y. Huang, L. Cui, Y. Xue, S. Zhang, N. Zhu, J. Liang, G. Li, *Mat Sci Eng. C.* **77**, 8 (2017). <https://doi.org/10.1016/j.msec.2017.03.253>
36. A. Mondal, N.R. Jana, *Chem. Commun.* **48**, 7318 (2012). <https://doi.org/10.1039/C2CC33410K>
37. M. Martín, P. Salazar, R. Álvarez, A. Palmero, C.L. Santos, J.L.G. Mora, A.R.G. Elipe, *Sensor Actuatos B.* **240**, 45 (2017). <https://doi.org/10.1016/j.snb.2016.08.092>
38. A. Safavi, F. Farjami, *Biosens. Bioelectron.* **26**, 2552 (2011). <https://doi.org/10.1016/j.bios.2010.11.002>